ISSN 1726-5749

SENSORS & TRANSDUCERS

vol. 90 Special 4/08

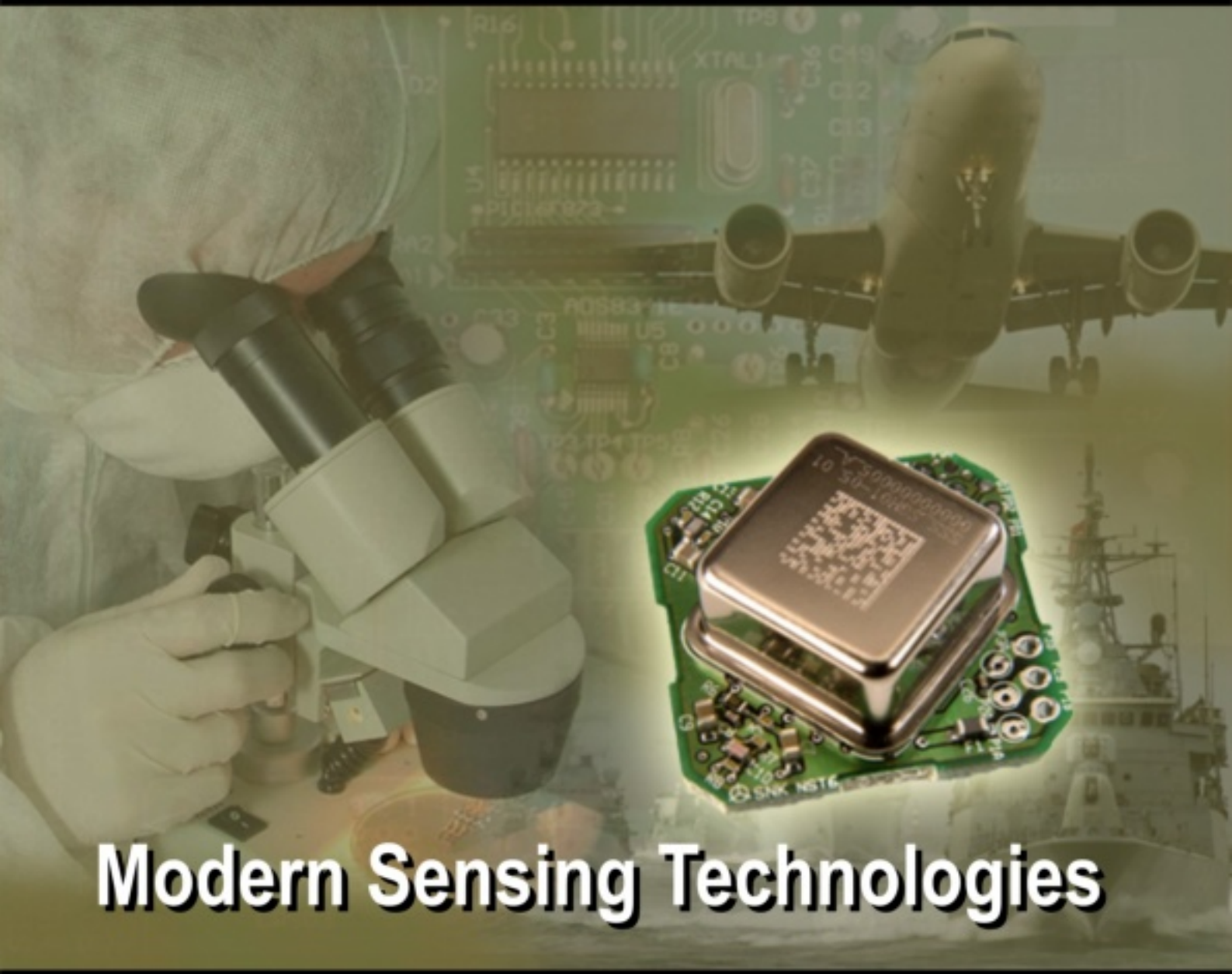

Modern Sensing Technologies

International Frequency Sensor Association Publishing

IFSA

Sensors & Transducers

Special Issue
April 2008

www.sensorsportal.com

ISSN 1726-5479

Sensors & Transducers Journal (ISSN 1726-5479) is a peer review international journal published monthly online by International Frequency Sensor Association (IFSA). Available in electronic and CD-ROM.

Sensors & Transducers Journal

Contents

Volume 90
Special Issue
April 2008

www.sensorsportal.com

ISSN 1726-5479

Special Issue on Modern Sensing Technologies

Editorial

Modern Sensing Technologies
Subhas Chandra Mukhopadhyay and Gourab Sen Gupta I

Sensors for Medical/Biological Applications

Characteristics and Application of CMC Sensors in Robotic Medical and Autonomous Systems
X. Chen, S. Yang, H. Natuhara K. Kawabe, T. Takemitu and S. Motojima 1

SGFET as Charge Sensor: Application to Chemical and Biological Species Detection
T. Mohammed-Brahim, A.-C. Salaün, F. Le Bihan 11

Estimation of Low Concentration Magnetic Fluid Weight Density and Detection inside an Artificial Medium Using a Novel GMR Sensor
Chinthaka Gooneratne, Agnieszka Łekawa, Masayoshi Iwahara, Makiko Kakikawa and Sotoshi Yamada 27

Design of an Enhanced Electric Field Sensor Circuit in 0.18 µm CMOS for a Lab-on-a-Chip Bio-cell Detection Micro-Array
S. M. Rezaul Hasan and Siti Noorjannah Ibrahim 39

Wireless Sensors

Coexistence of Wireless Sensor Networks in Factory Automation Scenarios
Paolo Ferrari, Alessandra Flammini, Daniele Marioli, Emiliano Sisinni, Andrea Taroni 48

Wireless Passive Strain Sensor Based on Surface Acoustic Wave Devices
T. Nomura, K. Kawasaki and A. Saitoh 61

Environmental Measurement OS for a Tiny CRF-STACK Used in Wireless Network
Vasanth Iyer, G. Rammurthy, M. B. Srinivas 72

Ubiquitous Healthcare Data Analysis And Monitoring Using Multiple Wireless Sensors for Elderly Person
Sachin Bhardwaj, Dae-Seok Lee, S.C. Mukhopadhyay and Wan-Young Chung 87

Capacitive Sensors

Resistive and Capacitive Based Sensing Technologies
Winncy Y. Du and Scott W. Yelich 100

A Versatile Prototyping System for Capacitive Sensing
Daniel Hrach, Hubert Zangl, Anton Fuchs and Thomas Bretterklieber 117

The Physical Basis of Dielectric Moisture Sensing
J. H. Christie and I. M. Woodhead 128

Sensors Signal Processing

Kalman Filter for Indirect Measurement of Electrolytic Bath State Variables: Tuning Design and Practical Aspects
Carlos A. Braga, Joâo V. da Fonseca Neto, Nilton F. Nagem, Jorge A. Farid and Fábio Nogueira da Silva 139

Signal Processing for the Impedance Measurement on an Electrochemical Generator
El-Hassane Aglzim, Amar Rouane, Mustapha Nadi and Djilali Kourtiche 150

Gas Sensors

Gas Sensing Performance of Pure and Modified BST Thick Film Resistor
G. H. Jain, V. B. Gaikwad, D. D. Kajale, R. M. Chaudhari, R. L. Patil, N. K. Pawar, M. K. Deore, S. D. Shinde and L. A. Patil 160

Zirconia Oxygen Sensor for the Process Application: State-of-the-Art
Pavel Shuk, Ed Bailey, Ulrich Guth 174

Image Sensors

Measurement of Digital Camera Image Noise for Imaging Applications
Kenji Irie, Alan E. McKinnon, Keith Unsworth, Ian M. Woodhead 185

Calibration-free Image Sensor Modelling Using Mechanistic Deconvolution
Shen Hin Lim, Tomonari Furukawa 195

Miscellaneous

Functional Link Neural Network-based Intelligent Sensors for Harsh Environments
Jagdish C. Patra, Goutam Chakraborty and Subhas Mukhopadhyay 209

MEMS Based Pressure Sensors – Linearity and Sensitivity Issues
Jaspreet Singh, K. Nagachenchaiah, M. M. Nayak 221

Slip Validation and Prediction for Mars Exploration Rovers
Jeng Yen 233

Actual Excitation-Based Rotor Position Sensing in Switched Reluctance Drives
Ibrahim Al-Bahadly 243

A Portable Nuclear Magnetic Resonance Sensor System
R. Dykstra, M. Adams, P. T. Callaghan, A. Coy, C. D. Eccles, M. W. Hunter, T. Southern, R. L. Ward 255

A Special Vibration Gyroscope
Wang Hong-wei, Chee Chen-jie, Teng Gong-qing, Jiang Shi-yu 267

An Improved CMOS Sensor Circuit Using Parasitic Bipolar Junction Transistors for Monitoring the Freshness of Perishables
S. M. Rezaul Hasan and Siti Noorjannah Ibrahim 276

Sensing Technique Using Laser-induced Breakdown Spectroscopy Integrated with Micro-droplet Ejection System
Satoshi Ikezawa, Muneaki Wakamatsu, Joanna Pawłat and Toshitsugu Ueda 284

A Forward Solution for RF Impedance Tomography in Wood
Ian Woodhead, Nobuo Sobue, Ian Platt, John Christie..... 294

A Micromachined Infrared Senor for an Infrared Focal Plane Array
Seong M. Cho, Woo Seok Yang, Ho Jun Ryu, Sang Hoon Cheon, Byoung-Gon Yu, Chang Auck Choi..... 302

Slip Prediction through Tactile Sensing
Somrak Petchartee and Gareth Monkman..... 310

Broadband and Improved Radiation Characteristics of Aperture-Coupled Stacked Microstrip Antenna for Mobile Communications
Sajal Kumar Palit 325

The Use of Bragg Gratings in the Core and Cladding of Optical Fibres for Accurate Strain Sensing
Ian G. Platt and Ian M. Woodhead 333

Authors are encouraged to submit article in MS Word (doc) and Acrobat (pdf) formats by e-mail: editor@sensorsportal.com
Please visit journal's webpage with preparation instructions: http://www.sensorsportal.com/HTML/DIGEST/Submition.htm

Sensors & Transducers Journal, Vol. 90, Special Issue, April 2008, pp. 233-242

www.sensorsportal.com

Sensors & Transducers

ISSN 1726-5479

http://www.sensorsportal.com

Slip Validation and Prediction for Mars Exploration Rovers

Jeng Yen
Jet Propulsion Laboratory, California Institute of Technology
Pasadena, California, USA
E-mail: Jeng.Yen@jpl.nasa.gov

Received: 15 October 2007 /Accepted: 20 February 2008 /Published: 15 April 2008

Abstract: This paper presents a novel technique to validate and predict the rover slips on Martian surface for NASA's Mars Exploration Rover mission (MER). Different from the traditional approach, the proposed method uses the actual velocity profile of the wheels and the digital elevation map (DEM) from the stereo images of the terrain to formulate the equations of motion. The six wheel speed from the empirical encoder data comprises the vehicle's velocity, and the rover motion can be estimated using mixed differential and algebraic equations. Applying the discretization operator to these equations, the full kinematics state of the rover is then resolved by the configuration kinematics solution in the Rover Sequencing and Visualization Program (RSVP) [1, 6, 10]. This method, with the proper wheel slip and sliding factors, produces accurate simulation of the Mars Exploration rovers, which have been validated with the earth-testing vehicle. This computational technique has been deployed to the operation of the MER rovers in the extended mission period. Particularly, it yields high quality prediction of the rover motion on high slope areas. The simulated path of the rovers has been validated using the telemetry from the onboard Visual Odometry (VisOdom) [2]. Preliminary results indicate that the proposed simulation is very effective in planning the path of the rovers on the high-slope areas. *Copyright © 2008 IFSA.*

Keywords: MER, Mars Rover, multi-body simulation, configuration kinematics, autonomous navigation

1. Introduction

In January 2004, NASA Mars Exploration Rover mission successfully landed two robot geologists: Spirit and Opportunity, on the surface of Mars. The mission's primary objective is to find evidence of past water on two sites: Gusev Crater and Meridiani Planum, on the opposite sides of the planet. In

over four year's operation of the MER vehicles, they have succeeded in the primary goal and are still roaming on the Martian surface for additional scientific targets. This tremendous achievement owes to the ability of the on-board mobility and the sequence simulation for planning safe path for the rovers in the harsh Martian surface. In this paper, we'll present the novel simulation scheme that enables the operation of the rovers.

Simulations of space-borne systems have been well developed and successfully applied to many of the past and current NASA missions. The modelling and simulation of spacecraft has been carried out using multi-body system dynamics [4]. The design and operation of the spacecraft are based on the predicted behavior using high-fidelity simulation tools [5] to carry out fly-by and other trajectory following activities. The surface operation of the robotic vehicles such as MER is, however, very different from those of traditional spacecraft operations. The most important aspect of the rover's simulation is the need to interact with the surrounding terrain. Based on the knowledge of the terrain, the simulator will predict the states of the rover. This requires effective modelling of the rover- terrain interaction. In addition, the multi-body rover model should include all the motorized mechanisms that are commandable for a comprehensive sequence simulation.

Rover sequencing and Visualization Program (RSVP) provides the capability to operate and control the MER rovers. Typically, the rovers are commanded once per Martian day, called a sol. A sequence of commands sent in the morning to specify the sol's activities: what images and data to collect, how to position the robotic arm, or where to drive. At the end of each sol, the rovers send back the data and images human operators will use to plan the next sol's activities. Using the command-level editing and the sequence-level simulation of RSVP, the operators can select the next sol's mobility commands and visualize the predicted motion [6, 8].

The sequence rehearsal tool in RSVP is based on modelling and simulation of the multi-body mechanical systems [10]. The methodology has been developed to support a real-time interactive graphics mode for the visualization tool, using the configuration kinematics algorithm [3] and a 3D terrain models. The sequence simulation is carried out using the on-board flight software modules for realistic rover behavior. Determined by the solution of six wheel-terrain contact equations, the algorithm solves the vehicle's wheels, steering and suspension linkages, and the position and orientation of the chassis. It treats the underlying mathematical model as an inverse-kinematics problem, and carries out the solutions using the computational techniques for constrained optimization. In this framework, the objective functions are comprised of three conditions: the rover's internal differential mechanisms, the wheel-terrain contact, and the commanded rover location and heading as shown in [3].

During the surface mission phase, the configuration kinematics simulation has provided fast and quality results for path planning on relatively level ground. The simulation results of the rover position and orientation using terrain DEM from the acquired images are remarkablely close to those of the on-board estimation [8]. But on steep hillsides, in mixed sand/rock terrains inside craters, and even when crossing sandy ripples in the otherwise flat plains of Meridiani, the simulation has not, as expected, been able to accurately predict the rover position due to large slips. The only on-board sensor that can detect position slip is the Visual Odometry (VisOdom) [2]. The VisOdom software compares two pairs of images to detect and track a set of features between these images. The motion of the features is used to update the vehicle's on-board position estimate according to the algorithm described in [9, 13]. On high-slip areas, the VisOdom can produce accuracy onboard position estimation, and has become a critical component of rover's safety systems. The telemetry of this onboard position will be used to validate the proposed slip model.

Conventional simulation of wheeled vehicles often uses a contact compliance formulation to deal with the complex wheel-terrain surface contact model [4]. A linear spring-damper actuator represents the

contact forces on the wheel. Based on the penetrative distance between the terrain and the wheel, a force will be applied to the vehicle's equations of motion to generate the dynamical effects from the contact. However, the numerical solutions of this dynamical system suffers from the instability and because the rough terrain profile and the physical limits of the linkages (e. g., the bumper-stops) can inject impulsive forces in such systems. All these modelling and numerical difficulties prevent a novel solution that achieves the real-time simulation of the rover traversal on a rocky terrain.

To overcome these difficulties a set of simplified dynamic equations is first developed and then heuristic wheel-ground speed estimation is applied to reduce the contact dynamics to a pseudo-dynamics for the slip model. This technique has been implemented in RSVP to compute ARC and TURN for MER vehicles. In the following section, we'll present the underlying framework of the MER vehicle simulation.

2. Mars Rovers Simulation

In RSVP, the MER vehicle model is represented by a set of hierarchical sub-graphs of the mechanism models for the primary motion systems. These sub-graphs are the foundation block for receiving sensed data, interpreting commands and predicting the physical states of the corresponding mechanical systems as shown in Fig. 1. The mobility mechanism consists of the Rocker-Bogey-Differential (RBD) suspension and the four-wheel steering systems. In Fig. 1, the suspension and the rover's kinematics, e.g., position and attitude, comprise a multi-body system of 10 states. These are the basic states of the rover's model for mobility. Note that six wheels with four steering motors comprise additional states of the full vehicle system, but these actuators are fully controlled by the onboard mobility software. Thus, the steering and driving motors are not accounted by the RSVP rover simulation model. In particular, the onboard mobility software controls the drive motors following a specific velocity profile to achieve the Ackermann steering on the flat ground [9].

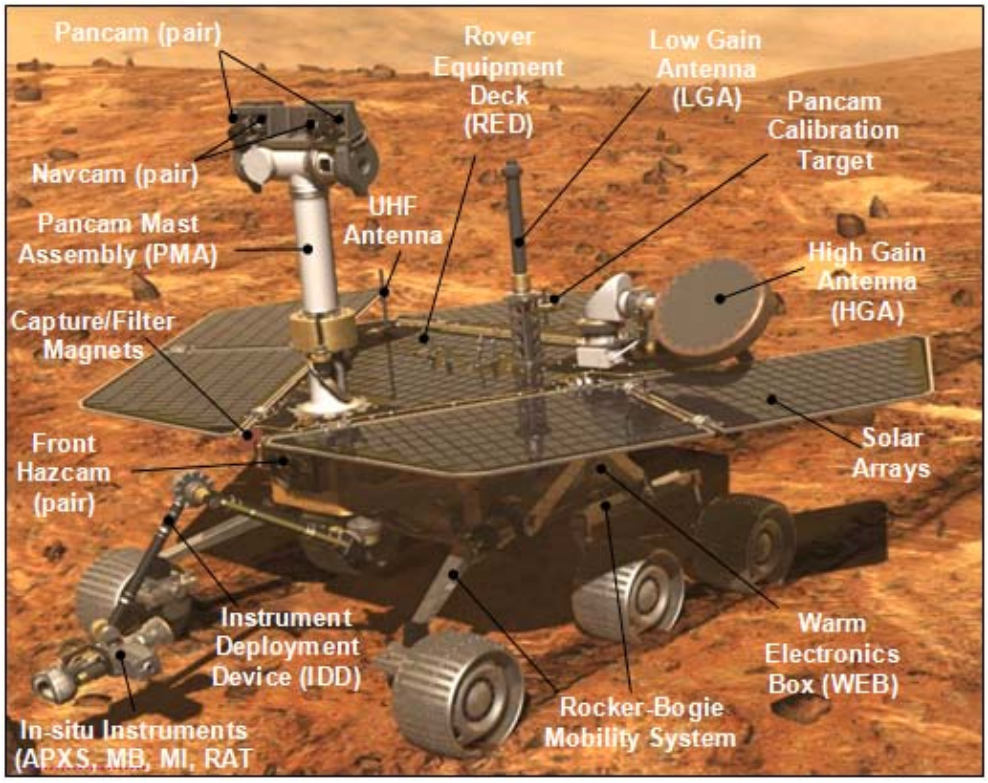

Fig. 1. Mars Exploration Rover.

The equations of motion of multi-body dynamic systems can be written as

$$\begin{aligned} \ddot{q} &= M^{-1}[f - G^T \lambda] \\ g(q) &= 0 \end{aligned}, \tag{1}$$

where q is the generalized coordinates, $\dot{q}$ and $\ddot{q}$ are the velocity and acceleration of the generalized states, M is the generalized mass matrix, f is the applied force, g is the algebraic constraint and $G = \frac{d}{dq} g$ is the Jacobian of the constraint, and $G^T \lambda$ represents the constraint reaction force, where λ is the Lagrange multiplier. The generalized coordinates q of the MER vehicles consist of 10 states, the vehicle's position and orientation, joint angles of the left and right rockers, and those of bogeys. The constraints g contains a linear equation of the differential, e.g., the joint angles of the left and right rockers are equal and have the opposite sign, and six rigid contact equations $g_{contact}(q) = dist(w,c) = 0$, where the distance of wheel centre to the terrain is equal to the wheel radius. Thus, Eq. 1 represents a system of only three degrees of freedom.

The solution of Eq. 1 can be obtained using the standard methods for Differential-Algebraic Equations (DAE) [11, 12], where a class of the discretization operators is directly applied to the differential part of Eq. 1. The stability of the solution in this approach often imposes a restricted stepsize of the discretization methods because of the so-called *artificial stiffness*. Alternatively, Eq. 1 can be rewritten to a state-space form, e.g., a set of differential equations representing the true degree of freedom in the system. One of these reduction techniques is the generalized coordinate partitioning method [4] that has been widely used in the simulation of ground vehicles in the automotive industry.

The state-space representation of the rover motion of (1) can be expressed as

$$\begin{aligned} \ddot{x} &= X^T M^{-1}[f - G^T \lambda] = f_x \\ \ddot{y} &= Y^T M^{-1}[f - G^T \lambda] = f_y \\ \ddot{\theta} &= \Omega^T M^{-1}[f - G^T \lambda] = \tau_z \end{aligned}, \tag{2}$$

where $[x, y, \theta]$ are the rover x-coordinate, y-coordinate and heading, the projection operators are defined as $x = X^T q, y = Y^T q, \theta = \Omega^T q$. It is interesting to note that the closed form state-space representation of Eq. 2 for a general multibody dynamical system can be very difficult to obtain. The right-hand-side of Eq. 2 is often evaluated using the generalized acceleration in Eq. 1.

Applying the time integration operator to Eq. 2 yields the *independent coordinate* of q. Apply the solution of the independent coordinates; the *dependent coordinates* in q can be obtained by solving the constraint equations, e.g.,

$$\begin{aligned} x &= \int v_x dt = \iint f_x d^2 t \\ y &= \int v_y dt = \iint f_y d^2 t \\ \theta &= \int \omega_z dt = \iint \tau_z d^2 t \\ g(q) &= 0 \end{aligned} \tag{3}$$

where $[v_x, v_y, \omega_z]$ is the velocity of the generalized coordinates $[x, y, \theta]$. Apply directly the desired rover position from an ARC or a TURN command, Eq. 3 can be written as

$$\begin{aligned} x - x_{arc} &= 0 \\ y - y_{arc} &= 0 \\ \theta - \theta_{arc} &= 0 \\ g(q) &= 0 \end{aligned} \tag{4}$$

where $[x_{arc}, y_{arc}, \theta_{arc}]$ is the result of commanded location and heading. The solution of Eq. 4 is then obtained by a Newton-type iterative method. Regular Newton-type iteration requires that g is *smooth* (e.g. $g \in C^2$ has 2nd order derivatives) to ensure a fast convergence. This prerequisite of a robust convergence is violated since the roughness of the terrain has been embedded in the contact equations. When the rocker or bogey linkages reaching its limits, an abruption of the iteration can induce unpredictable solution of the configuration. To overcome these numerical difficulties, we applied a weight factor to the residual of each contact equation. During the iterations, the weight factor for a given wheel can be reduced to zero to relax the contact condition. Whenever the wheel leaves the ground, its corresponding weight factor is set to zero for a total relaxation of this wheel-terrain contact. The re-scaling of the weight factors is coupled with the global search algorithm, which can detect the joint limits associated with each wheel-terrain contacts, and can sample small perturbations around the contacting locations to determine the occurrence of a separation of the wheel and the ground.

The step-selection strategy used in the global search is a backtracking line search algorithm that monitors the progress of the iteration. For a smooth terrain profile, the iterative solution generated by the Newton method converges very rapidly to a local minimum of the nonlinear equations. However, the rate of convergence can be tremendously decreased when a non-smooth terrain profile appears. Special care is taken to maintain robust and efficient solution in the case of a non-smooth terrain profile. Although the problem in hand is ill posed (i.e., it is well-known that the Newton method cannot treat non-smooth equations), we developed a heuristic solution to ease the computational difficulty in the iterations. In practice, the wheel-terrain contact is treated as a non-penetrative type, which is not a realistic portrait of the nature wheel-terrain interaction. Therefore, a search direction to the wheel-terrain contact may not in-line with the normal direction of the terrain (at the contact location), instead; it could be anywhere along the perimeter of the wheel. The heuristic leads to modelling the wheel-terrain contact equation as the distance constraint between the wheel centre and the terrain profile. On the level ground, the solution of Eq. 3 by the aforementioned techniques results in an efficient and accuracy estimation of the commended location of the MER vehicles [6, 10].

Equation 3 can be again re-written as first-order differential-algebraic equations by applying the time differentiation operator to the state variables $[x, y, \theta]$ of Eq. 4. This yield

$$\begin{aligned} \dot{x} - v_x &= 0 \\ \dot{y} - v_y &= 0 \\ \dot{\theta} - \omega_z &= 0 \\ g(q) &= 0 \end{aligned} \tag{5}$$

In fact, Eq. 5 can also be obtain from Eq. 4 if we declare that the time derivatives are $v_x = \frac{d}{dt} x_{arc}$, $v_y = \frac{d}{dt} y_{arc}$, and $\omega_z = \frac{d}{dt} \theta_{arc}$. The vehicle's speed when performing the ARC and TURN has been measured in the earth-testbed, so these empirical vehicle speed profiles/tables may be used directly in

Eq. 5. A straightforward calculation leads to the "slip tables" approach that uses only the empirical data to approximate the slips. Then the modified Eq. 3 is resolved for the add-on slips. However, only these tables can represent the gross motion, and the dimension of these tables can be very large.

Using the rigid-body motion, the velocity of the independent states can be obtained from a consistent wheel-ground speed. Since the onboard drive motor controller is always keeping up with a pre-defined profile, we can use the speed profile and the local terrain geometry for an approximated velocity of the independent variables. Moreover, the wheel-terrain slip can be incorporated in this approximation so that the vehicle total slip can be computed accordingly. A heuristic approach is to "average" the wheel-ground speed of each wheel for the independent velocity $[v_x, v_y, \omega_z]$. Let the $i-th$ wheel's velocity projected onto the plane interpolation of the terrain patch under the wheel be

$$v_i^W = (I - P_i P_i^T)\bar{v}_i^W, \tag{6}$$

where $(I - P_i P_i^T)$ is the projection and $\bar{v}_i^W$ is the nominal wheel speed. Assuming the rigid contact condition, the wheel-ground speed is along the tangential direction of the contact plane, as shown in Eq. 6. For all six wheels in contact with ground, the rover velocity is a linear combination of the wheel-ground velocity, e.g., vehicle's velocity is within the convex hull of all the wheel velocity. Apply the partitioning operator and a weight factor to each of the driving wheels yields

$$\begin{aligned} v_x &= X^T(\sum_i \frac{\alpha}{6}(1+s_i)v_i^W + \beta\delta_x) \\ v_y &= Y^T(\sum_i \frac{\alpha}{6}(1+s_i)v_i^W + \beta\delta_y) \\ \omega_z &= \Omega^T \sum_i \frac{1}{3}\left(r_i \times v_i^W\right) \end{aligned} \tag{7}$$

where $\alpha \in [0,1]$ and $\beta \in [0,1]$represent the weight factors, and r_i is the location of the wheel in the rover's navigation frame, $s_i \in [-1,1]$ is the wheel-slip model parameter, and the sliding vector

$$\delta = \begin{bmatrix} \delta_x \\ \delta_y \end{bmatrix} = \frac{1}{\|\bar{v}\|}\left(I - PP^T\right)\bar{v}, \tag{8}$$

where $\bar{v} = \sum_i \frac{1}{n}(I - P_i P_i^T)v_i^W$ is the nominal rover speed. Typically, the sliding vector is along the down slope direction on a local patch of the terrain where the vehicle is treated as a point-mass on a gravitational field, representing the gravitational forces acting on the independent coordinates (x, y), respectively. Using Eqs. 5 and 7, the rover position and orientation, and the joint angles of the rockers and bogeys can be obtained. The weight factor is selected based on the local geometry, e.g., the *wheel-ground angle*. The magnitude of sliding vector is determined by the experimental data of the slip tables. Since the maximum tilt of the static stable configuration of the MER vehicles is 35 degrees, the weight factor and sliding factor are obtained from the results interpolated between 0 to 30 degrees.

3. Results

The numerical test for the rover slip model is illustrated by Figs. 2-5 using a synthetic terrain. The rover started at the origin (0, 0) of a 14-degrees slope. The testing sequence comprised of a 3-meter ARC driving downhill, then a 3-meter ARC back up to the origin, then TURN to 0 degree heading, then driving forth and back with two 3-meter ARCs. Comparing the "no slip" simulation using Eq. 4, with the simulation using Eq. 5 and 7, the slippage predicted by the simulation matches well with those of the experiments.

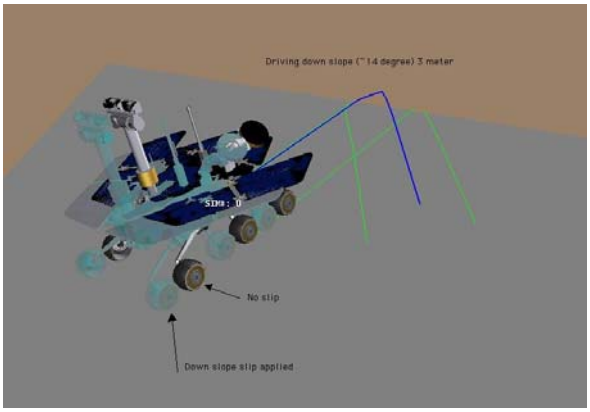

Fig. 2. Down Slope Driving 14% Slip.

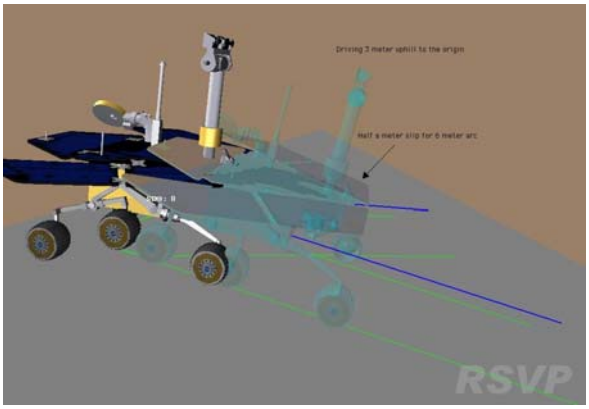

Fig. 3. Up Slope Driving 14-16% Slip.

Fig. 2 shows a 14% down-slope slip of the straight arc. The uphill straight arc illustrated in Fig. 3 shows a similar down-slope slide. In Fig. 4 and 5, the forward and back arcs driving on the side-slope also slide toward the down-slope direction at about 10 % of the traveling distance.

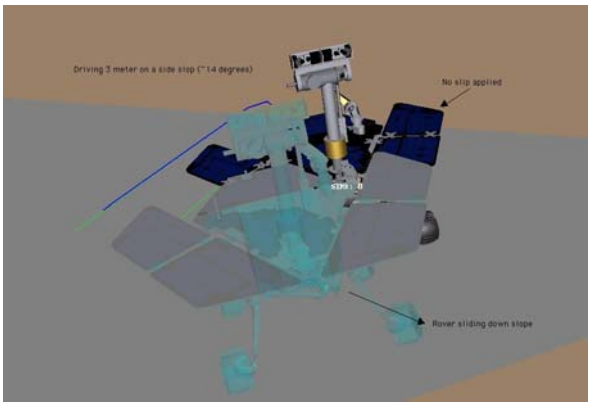

Fig. 4. Side Slope Driving 10% Slip.

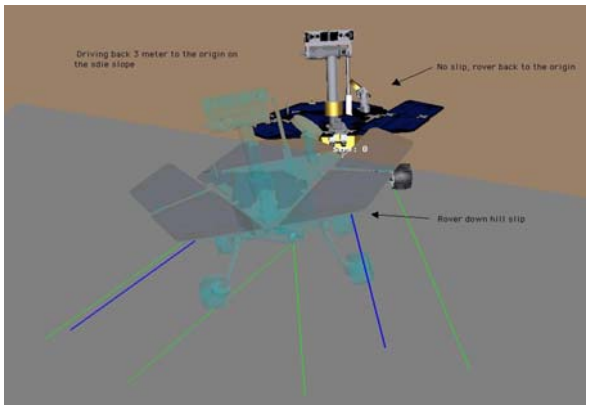

Fig. 5. Side Slope Driving 10% Slip.

The simulation results matched well with the results of the test-bed vehicle. In fact, the slip and sliding parameters of the rover slip model, e.g., $\alpha \in [0,1]$ and $\beta \in [0,1]$ in Eq. (7), are defaulted to the earth-vehicle's performance on the test-bed ramp. When applied the slip model for the MER drives, the slip and sliding parameters can be adjusted to fit different type of surface textures.

We learned during our initial drives in each terrain that driving on level ground typically leads to accurate and predictable mobility performance; e.g., Spirit only accumulated 3% position error over 2

kilometers of driving [8]. Before driving into Endurance Crater, a series driving tests were carried out to establish a set of slip tables for MER vehicles. These tables measure the slippage percentage based on the tilt angle of the vehicle assuming a flat surface underneath. We have implemented the slip tables in RSVP simulation as the baseline method to compute the weight factors in Eq. 7. From the test results, the vehicle exhibits about 1 % slip (of the total driving distance) per degree on a slope ranging 10-20 degrees sandy surface. Similar performance on the MER vehicles when driving on the Martian surface covered with “blue berries”, that is a small grind of round pebbles.

While most of the distance covered by the rovers was on level ground, most of the sols and most of the approach drive occurred on slopes. The rovers invariably slip when driving on slopes, making VisOdom essential for safe and accurate driving. To construct a successful drive on high slope areas, accurate estimation of the commanded location can only be obtained with the correct vehicle slips. On sol 1329, Opportunity drove inside the **Victoria Crater** approaching the science target located on layered outcrop as shown in Fig. 6 indicated by the green clover at the lower left corner. Blue lines in the pictures represent the path of the rover centre while the green lines are the track of the middle wheels, and the red lines enclosed the “keep-out zoom” where the drive will be halted if the rover centre entered.

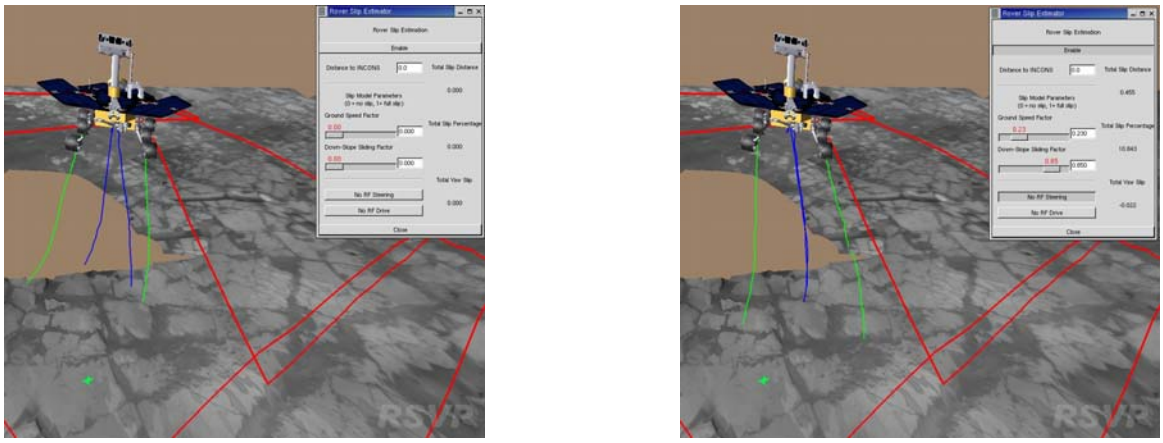

Fig. 6. Inside Victoria Crater without (left) vs. with (right) the slip model.

The planned path is 4.4 meters as shown in Fig. 6. With no slip model, the predicted path and the onboard VisOdom estimation differed by about 0.5 meters, a total slip of 10%. The predicted path using the slip model is shown in the right picture of the Fig. 6. Using α=0.23 and β = 0.81 the simulated path matches well with the actual rover motion. Note that the slope of this course is between 16 t0 19 degrees.

Endurance Crater

Another validation of this modeling technique is the Opportunity drive on sol 304, where the goal is to place the science targets into the rover’s robotic arm’s work volume. The rover drove 8 meters west and gained 0.9 meters in elevation using VisOdom on the slope about15-18 degrees. VisOdom maintained the on-board position knowledge during the drive, while the rover drivers planned the sequence with preempted corrections. In Fig. 7, the simulated paths with and without the slip model are compared with the on-board VisOdom estimated path. It is cleared that the slip model produces a better prediction.

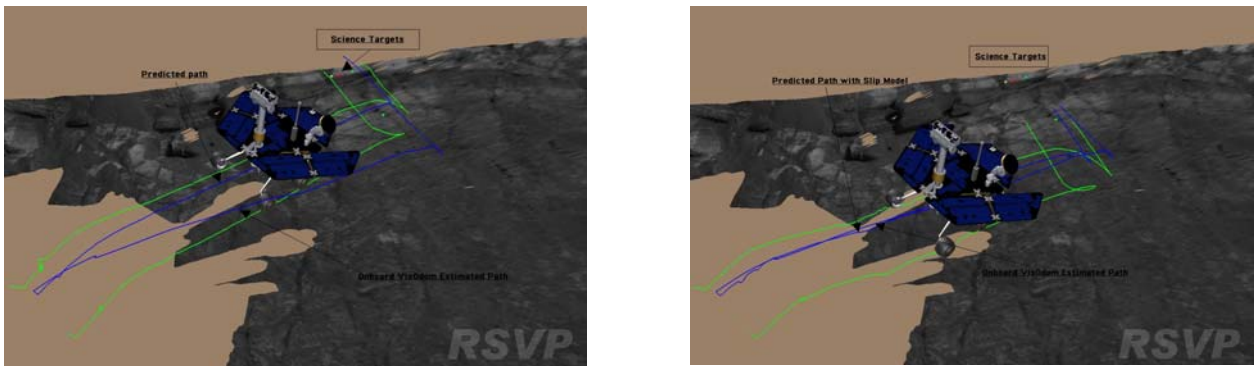

Fig. 7. Endurance Crater without Slip (left) and with 14 % Slip (right).

4. Conclusions

The proposed slip model for the Mars Exploration Rovers is an effective tool to predict and validate the mobility of the rovers. Using the wheel velocity, the model, derived from a simplified vehicle dynamics, computes an accurate vehicle slippage based on the terrain geometry. To date, the slip model has been used in the daily basis to command the MER rovers driving in the Martian environment.

Acknowledgements

Thanks to Jeff Biesiadecki for insightful discussion on the motor controller onboard the MER flight system, RSVP team lead Brian Cooper and the team members (Frank Hartman, Scott Maxwell, and John Wright) for supporting the inclusion of the slip model in RSVP, Mark Maimone for fruitful discussion on validating the slip model using the telemetry and VisOdom data.

The work described in this paper was carried out at the Jet Propulsion Laboratory, California Institute of Technology, under a contract to the National Aeronautics and Space Administration. Copyright 2008 California Institute of Technology. Government sponsorship acknowledged.

References

[1]. B. Cooper, F. Hartman, S. Maxwell, and J. Wright, J. Yen, Using RSVP for Analyzing State and Previous Activities for the Mars Exploration Rovers, In *SpaceOps*, Montreal, Canada, 2004.
[2]. Yang Cheng, Mark Maimone, and Larry Matthies, Visual odometry on the Mars Exploration Rovers, In *IEEE Conference on Systems, Man and Cybernetics*, The Big Island, Hawaii, USA, October 2005.
[3]. J. Yen, A. Jain and B. Balaram, ROAMS: Rover Analysis, Modeling and Simulation, In *the Proc. of 5th iSAIRAS*, ESA, Netherland, 1999.
[4]. E. J. Haug, Computer Aided Kinematics and Dynamics of Mechanical Systems, *Allyn-Bacon*, 1989.
[5]. Biesiadecki J., Henriquez D., and Jain A., A Reusable, Real-Time Spacecraft Dynamics Simulator, *Proceedings of the Sixth Digital Avionics Systems Conference*, Irvine, CA, October 1997.
[6]. S. Maxwell, et. al, The best of both worlds: Integrating textual and visual command interfaces for mars rover operations, in *Proc. IEEE Syst., Man, Cybern. Conf.*, 2005, Vol. 2, pp. 1384–1388.
[7]. Rongxing Li, et al. Spirit rover localization and topographic mapping at the landing site of Gusev Crater, Mars, JGR-Planets, *Special Issue on Spirit Rover*, 111 (E02S06, doi: 10.1029/2005JE002483). http://www.agu.org/journals/ss/SPIRIT1/
[8]. Mishkin A. H., Limonadi D., Laubach S. L., Bass D. S., Working the Martian night shift - the MER surface operations process, *Robotics & Automation Magazine*, IEEE, Vol. 13, Issue 2, June 2006, pp. 46 – 53.

[9]. Biesiadecki J. J., Leger P. C. and Maimone M. W., Tradeoffs between directed and autonomous driving on the Mars Exploration Rovers, *International Journal of Robotics Research*, 26, 1, 2007, pp. 91–104.
[10]. J. Yen, B. Cooper, F. Hartman, S. Maxwell and J. Wright, Sequence rehearsal and validation on surface operations of the Mars Exploration Rovers, In *SpaceOps.*
[11]. E. J. Haug and J. Yen, Implicit Numerical Integration of Constrained Equations of Motion via Generalized Coordinate Partitioning, *ASME J. of Mechanical Design*, Vol. 114, June, 1992, pp. 296-304.
[12]. J. Yen and L. R. Petzold An Efficient Newton-Type Iteration for the Numerical Solution of Highly Oscillatory Constrained Multibody Dynamic Systems, *SIAM J. Sci. Stat. Comput*., Vol. 19, No. 5, Sept. 1998, pp. 1513-1534.
[13]. D. M. Helmick, S. I. Roumeliotis, Y. Cheng, D. Clouse, M. Bajracharya, L. Matthies, Slip-Compensated Path Following for Planetary Exploration Rovers, *Advanced Robotics*, Vol. 20, No. 11, November, 2006, pp. 1257-1280.

Guide for Contributors

Aims and Scope

Sensors & Transducers Journal (ISSN 1726-5479) provides an advanced forum for the science and technology of physical, chemical sensors and biosensors. It publishes state-of-the-art reviews, regular research and application specific papers, short notes, letters to Editor and sensors related books reviews as well as academic, practical and commercial information of interest to its readership. Because it is an open access, peer review international journal, papers rapidly published in *Sensors & Transducers Journal* will receive a very high publicity. The journal is published monthly as twelve issues per annual by International Frequency Association (IFSA). In additional, some special sponsored and conference issues published annually.

Topics Covered

Contributions are invited on all aspects of research, development and application of the science and technology of sensors, transducers and sensor instrumentations. Topics include, but are not restricted to:

- Physical, chemical and biosensors;
- Digital, frequency, period, duty-cycle, time interval, PWM, pulse number output sensors and transducers;
- Theory, principles, effects, design, standardization and modeling;
- Smart sensors and systems;
- Sensor instrumentation;
- Virtual instruments;
- Sensors interfaces, buses and networks;
- Signal processing;
- Frequency (period, duty-cycle)-to-digital converters, ADC;
- Technologies and materials;
- Nanosensors;
- Microsystems;
- Applications.

Submission of papers

Articles should be written in English. Authors are invited to submit by e-mail editor@sensorsportal.com 6-14 pages article (including abstract, illustrations (color or grayscale), photos and references) in both: MS Word (doc) and Acrobat (pdf) formats. Detailed preparation instructions, paper example and template of manuscript are available from the journal's webpage: http://www.sensorsportal.com/HTML/DIGEST/Submition.htm Authors must follow the instructions strictly when submitting their manuscripts.

Advertising Information

Advertising orders and enquires may be sent to sales@sensorsportal.com Please download also our media kit: http://www.sensorsportal.com/DOWNLOADS/Media_Kit_2008.pdf